





High quantum oscillation frequencies and nontrivial topology in kagome superconductor KV_3Sb_5 probed by torque magnetometry up to 45 T

K. Shrestha ^{1,*}, M. Shi,² B. Regmi,³ T. Nguyen,¹ D. Miertschin ¹, K. Fan,² L. Z. Deng ⁴, N. Aryal,⁵ S.-G. Kim,³ D. E. Graf,^{6,7} X. Chen,² and C. W. Chu ^{4,8}

¹Department of Chemistry and Physics, West Texas A&M University, Canyon, Texas 79016, USA

²Hefei National Laboratory for Physical Sciences at the Microscale, University of Science and Technology of China, Hefei 230026, China

³Department of Physics and Astronomy, Mississippi State University, Mississippi State, Mississippi 39762, USA

⁴Texas Center for Superconductivity and Department of Physics, University of Houston, 3369 Cullen Boulevard, Houston, Texas 77204-5002, USA

⁵Condensed Matter Physics and Materials Science Division, Brookhaven National Laboratory, Upton, New York 11973, USA

⁶Department of Physics, Florida State University, Tallahassee, Florida 32306, USA

⁷National High Magnetic Field Laboratory, Tallahassee, Florida 32310, USA

⁸Lawrence Berkeley National Laboratory, 1 Cyclotron Road, Berkeley, California 94720, USA



(Received 24 September 2022; revised 29 January 2023; accepted 3 April 2023; published 14 April 2023)

Here, we present the Fermi surface properties of the kagome superconductor KV_3Sb_5 using torque magnetometry at applied fields up to 45 T and temperatures down to that of liquid ^3He (0.32 K). The torque signal shows clear de Haas–van Alphen (dHvA) oscillations with 14 major frequencies ranging from ~ 33 to 2149 T, nine of which are higher frequencies (above 500 T) that have never been reported in KV_3Sb_5 . Angular dependence measurements of the dHvA oscillations were carried out to investigate the dimensionality of the Fermi surface. Based on our analysis, several frequencies follow the $1/\cos\theta$ dependence, where θ is the tilt angle with respect to the applied field direction and oscillations disappear above $\theta = 60^\circ$, which suggest that Fermi surfaces corresponding to these frequencies are quasitwo dimensional. The Berry phase (Φ_B), determined by constructing a Landau level fan diagram, was found to be $\Phi_B \sim \pi$, which strongly suggests the nontrivial topology of KV_3Sb_5 . To explain the experimental results, we carried out band-structure and Fermi-surface calculations using density functional theory (DFT) for both pristine and charge-density wave (CDW) phases. We found that the Fermi surface undergoes severe reconstruction in the CDW phase and, more importantly, our calculation results are in reasonable agreement with the experimentally measured Fermi-surface frequencies. The observation in this paper of very high quantum oscillation frequencies in KV_3Sb_5 and the determination of their detailed Fermi-surface properties, along with the analyses of corresponding DFT calculation results, are crucial for understanding CDW order, unconventional superconductivity, and nontrivial topology in AV_3Sb_5 ($A = \text{K, Rb, and Cs}$), as well as the interplay among them.

DOI: [10.1103/PhysRevB.107.155128](https://doi.org/10.1103/PhysRevB.107.155128)

I. INTRODUCTION

Recently, the discovery of kagome metals AV_3Sb_5 ($A = \text{K, Rb, and Cs}$) [1–3] has attracted significant interest in the study of condensed-matter physics as they provide fertile ground for exploring the interplay among charge-density wave (CDW) order, superconductivity, and nontrivial band topology. Several exotic quantum phenomena, including superconductivity ($T_c \sim 0.3\text{--}3$ K), CDW order near $T_{\text{CDW}} \sim (80\text{--}110$ K) [4–7], anomalous Hall effect [8,9], and a van Hove singularity [10] have been discovered in these materials. They possess several Dirac-like band crossings near the Fermi level [1–3] with a nonzero \mathbb{Z}_2 topological invariant. The observation of a robust zero-bias conductance peak in a tunneling experiment on CsV_3Sb_5 [11] suggests that

this compound could be an ideal candidate for topological superconductivity.

CDW order gradually disappears, whereas T_c shows an unusual M -shaped double dome with the application of external pressure [5,6]. These observations strongly suggest unusual interplay between CDW order and superconductivity of AV_3Sb_5 that needs to be investigated. In addition, time-reversal symmetry breaking and electronic nematicity have been revealed inside the triple- Q CDW state [12,13], implying that the nature of the CDW phase is unconventional. Therefore, a detailed knowledge of the Fermi surface would be invaluable for understanding the CDW phase and superconductivity in AV_3Sb_5 . There have been several Fermi surface studies [8–10,14–17] of these materials using both quantum oscillations and angle-resolved photoemission spectroscopy measurements. Based on the quantum oscillation measurements, only low oscillation frequencies (below 500 T) have been reported in AV_3Sb_5 . However, our recent high-field measurements [18] on CsV_3Sb_5 , along with studies by Ortiz

*kshrestha@wtamu.edu

et al. [16] and Fu *et al.* [19], have shown that there exist several higher frequencies with values reaching as high as 3000 T. The most recent quantum oscillations data [20–22] have shown even higher quantum oscillation frequencies up to 10 kT, as well as a very large effective mass (m^*) of the charge carriers $m^* \sim 2m_0$, where m_0 is the free-electron mass. The observation of such high frequencies in CsV_3Sb_5 is quite interesting, and their origin has yet to be understood. It has been argued that the CDW transition results in Fermi-surface reconstruction and that the high frequencies emerge from the reconstructed pockets [16,19]. Most Fermi-surface studies, especially those using quantum oscillation measurements, have focused on CsV_3Sb_5 . It would be intriguing to explore whether similar high frequencies exist in other members of the AV_3Sb_5 family (KV_3Sb_5 and RbV_3Sb_5) and how their Fermi surfaces would appear. There have only been a few quantum oscillation studies on KV_3Sb_5 [9] and RbV_3Sb_5 [14] to date, and only low frequencies below 500 T have been reported. Yang *et al.* [9] observed two frequencies (34.6 and 148.9 T) in KV_3Sb_5 using Shubnikov–de Haas (SdH) oscillations, but they did not provide the detailed Fermi-surface properties.

Here, we present details regarding the Fermi surface of one of the AV_3Sb_5 compounds, KV_3Sb_5 , determined using the torque magnetometry technique. The torque signal clearly shows de Haas–van Alphen (dHvA) oscillations with 14 distinct frequencies up to 2149 T. The angle-dependent data prove that these frequencies arise from quasi-two-dimensional (2D) Fermi-surface pockets. Our Berry phase analyses confirm the nontrivial topology of KV_3Sb_5 . Electronic structure calculations using density functional theory (DFT) were carried out to support the experimental data. A comparison between the experimentally determined frequencies and those calculated from DFT is presented.

II. EXPERIMENTAL DETAILS

High-quality single crystals of KV_3Sb_5 were synthesized using the self-flux method. The detailed procedures of the material synthesis, along with energy-dispersive x-ray spectroscopy analyses, are presented in the Supplemental Material [23] (Fig. S1 and Table S1). The KV_3Sb_5 crystal structure was characterized using an x-ray diffractometer (Rigaku SmartLab) equipped with Cu $K\alpha$ radiation and a fixed graphite monochromator. Magnetic susceptibility and electrical transport measurements were carried out using a superconducting quantum interference device magnetometer (Quantum Design, MPMS 5 T) and a physical property measurement system (Quantum Design, 9 T), respectively. High-field measurements were carried out at the National High Magnetic Field Laboratory in Tallahassee, FL. The magnetic torque was measured using a miniature piezoresistive cantilever as described in our previous publication [18]. We rotated the sample at different tilt angles (θ), where θ is the angle between the magnetic field and the c axis of the sample, under an applied field. The sample was maintained at a fixed θ during temperature-dependent magnetic torque measurements. Magnetic fields were swept at each fixed temperature at a rate of 2.2 T/min.

The DFT calculations were performed by using the Vienna *ab initio* simulation package (VASP) [24,25]. The Perdew-

Burke-Ernzerhof exchange-correlation functional [26] within the generalized gradient approximation was used in all the calculations. Full lattice relaxation was performed for both the pristine and the CDW ($2 \times 2 \times 1$ trigonal hexagonal) phases until the forces were less than 0.02 eV/Å. A plane-wave energy cutoff of 520 eV and an energy convergence criterion of 10^{-5} eV were used for both pristine and CDW ($2 \times 2 \times 1$) structures. γ -centered k grids with dimensions of $16 \times 16 \times 10$ (for the primitive cell) and $8 \times 8 \times 10$ (for the supercell) were used to sample the respective Brillouin zones. Band unfolding of the CDW phase into the undistorted phase was achieved using the method developed by Popescu and Zunger [27] as implemented in the VASPBANDUNFOLDING code [28]. The Fermi surfaces were generated using a dense k -point grid of $18 \times 18 \times 20$ and visualized using the XCRYSDEN software package [29]. The quantum oscillation frequencies were calculated using the SKEAF code [30].

III. EXPERIMENTAL RESULTS AND DISCUSSION

Figure 1(a) shows the room-temperature x-ray diffraction (XRD) pattern of a KV_3Sb_5 single crystal. The XRD peaks can be indexed to the hexagonal structure [space-group $P6/mmm$]. The presence of only peaks with Miller indices $(00l)$ ($l = 1-3, \dots$) implies that the c axis is perpendicular to the plane of the platelet (i.e., the ab plane). Figure 1(b) shows magnetic susceptibility (χ) vs temperature for KV_3Sb_5 measured under an applied field of 7 T along the c axis. A sharp anomaly appears in the $\chi(T)$ curve at $T_{\text{CDW}} \sim 80$ K as indicated by the arrow due to CDW order. The CDW transition is more visible in the inset to Fig. 1(b).

The temperature-dependent electrical resistivity (ρ) of KV_3Sb_5 from room temperature to 1.8 K is shown in Fig. 1(c). $\rho(T)$ decreases with decreasing temperature, showing typical metallic behavior. The residual resistivity ratio (RRR) = $\rho(300 \text{ K})/\rho(2 \text{ K})$ is found to be 19, which is almost half of the RRR value (~ 45) reported by Yang *et al.* [9]. Since the T_c value for KV_3Sb_5 is 0.93 K [2], the temperature range used for these measurements is not low enough to show the absence of electrical resistance resulting from superconductivity. It is important to note that, unlike in the magnetic susceptibility data [Fig. 1(b)], there is no clear indication of the CDW transition in the $\rho(T)$ data. Therefore, we have calculated the first derivative of $\rho(T)$, i.e., $d\rho/dT$ as shown in the inset of Fig. 1(c). An anomaly at $T_{\text{CDW}} \sim 80$ K resulting from CDW order is visible in the temperature-dependent $d\rho/dT$ results as indicated by the arrow. The T_{CDW} values in our magnetic susceptibility and resistivity measurements are comparable to one another and are consistent with those previously reported [1,3] for KV_3Sb_5 .

To investigate the Fermi surface of KV_3Sb_5 , we measured the magnetic torque (τ) for two KV_3Sb_5 single crystals K1 and K2 at applied fields up to 45 T and temperatures down to 0.32 K. Figure 2(a) shows τ vs H for K1 and K2 at 0.32 K. The τ signal increases with H and shows clear dHvA oscillations above 20 T. The quantum oscillations are visible in both K1 and K2, and we found that both samples have comparable frequency spectra (Fig. S2 in the Supplemental Material [23]). However, as seen in Fig. 2(a), the oscillations are more pronounced in K2 compared to those in K1. Therefore,

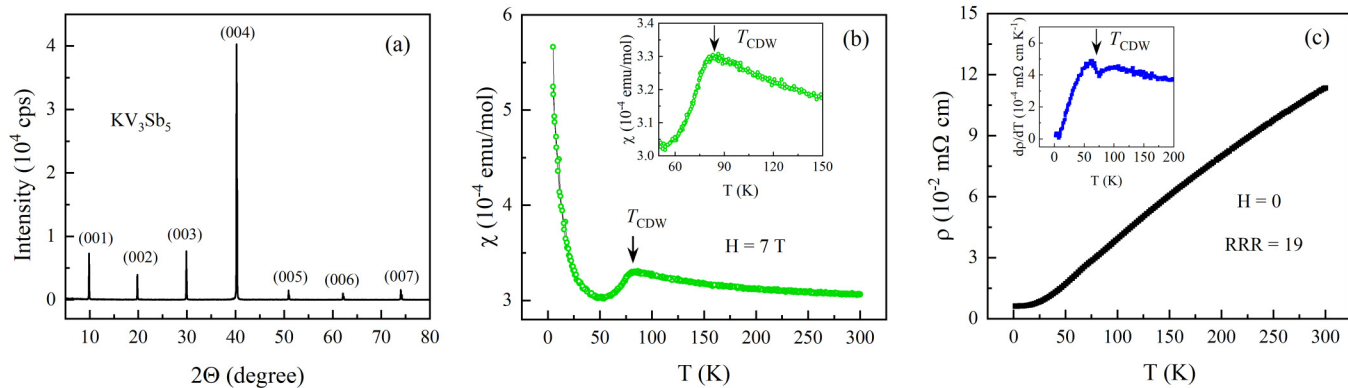


FIG. 1. XRD, magnetic susceptibility, and electrical resistivity. (a) Room-temperature XRD pattern of a KV_3Sb_5 single crystal indexed to the $P6/mmm$ structure. (b) Temperature-dependent magnetic susceptibility $\chi(T)$, measured by applying $H = 7$ T along the c axis. There is a clear anomaly in the $\chi(T)$ data near 80 K as indicated by the arrow. The inset: magnified view of $\chi(T)$ near the CDW transition (T_{CDW}). (c) In-plane electrical resistivity vs temperature, $\rho(T)$, for KV_3Sb_5 . $\rho(T)$ decreases with decreasing temperature, indicating typical metallic behavior. The residual resistivity ratio (RRR) value is found to be ~ 19 . The inset: first derivative of the $\rho(T)$ data showing $T_{CDW} \sim 80$ K.

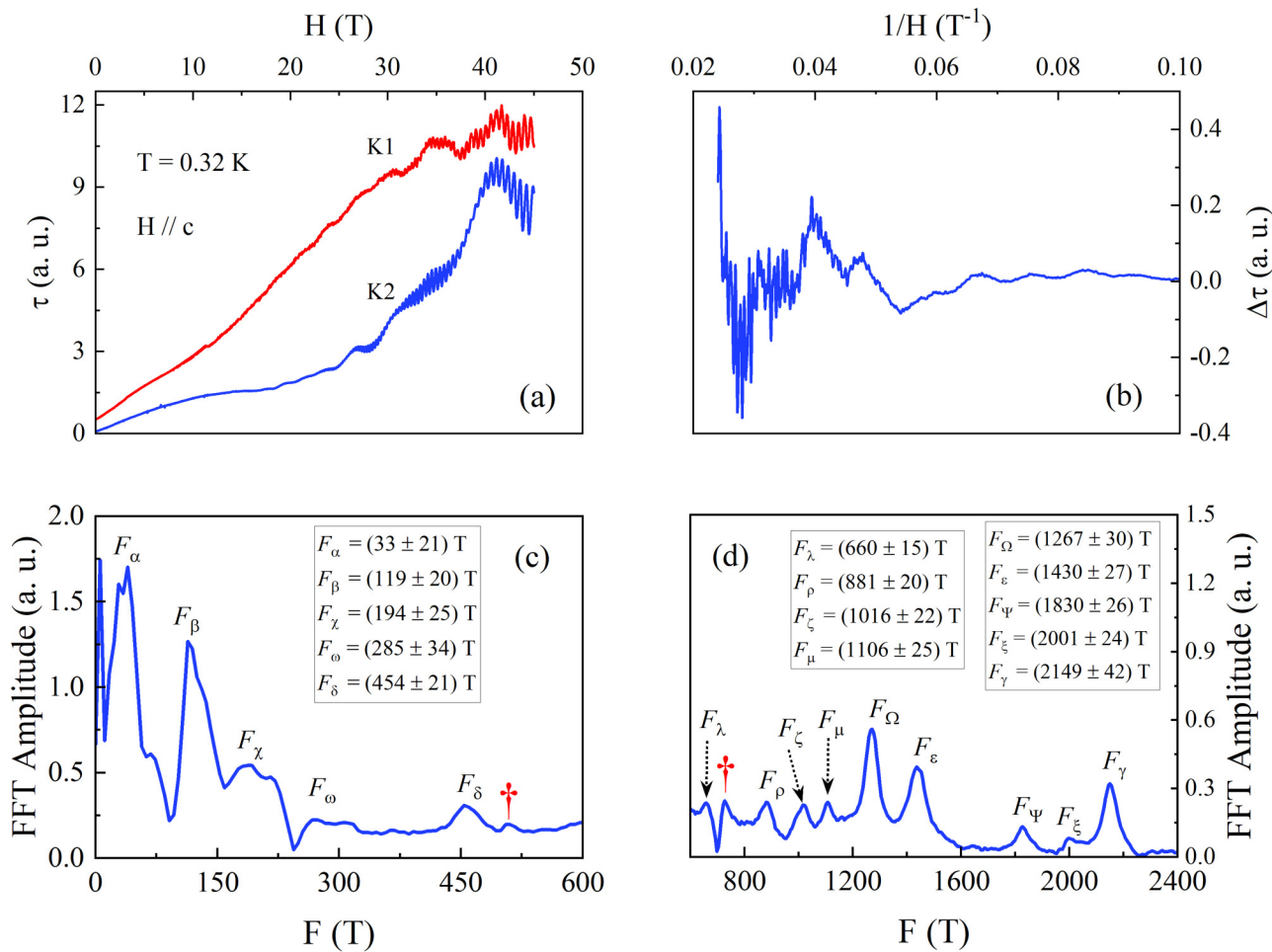


FIG. 2. dHvA oscillations and Fourier transform. (a) Magnetic torque for two KV_3Sb_5 single crystals (K1 and K2) measured at $T = 0.32$ K. Both samples show clear dHvA oscillations above 20 T. (b) Background-subtracted dHvA oscillations for K2 at $\theta = 0^\circ$. Fast Fourier transform (FFT) spectrum in the frequency ranges of (c) 0 to 600 T and (d) 600 to 2400 T. There are 14 labeled frequency peaks, nine of which are above 500 T. Some peaks in the spectrum as indicated by the daggers in (c) and (d) are not considered here (see the discussion below).

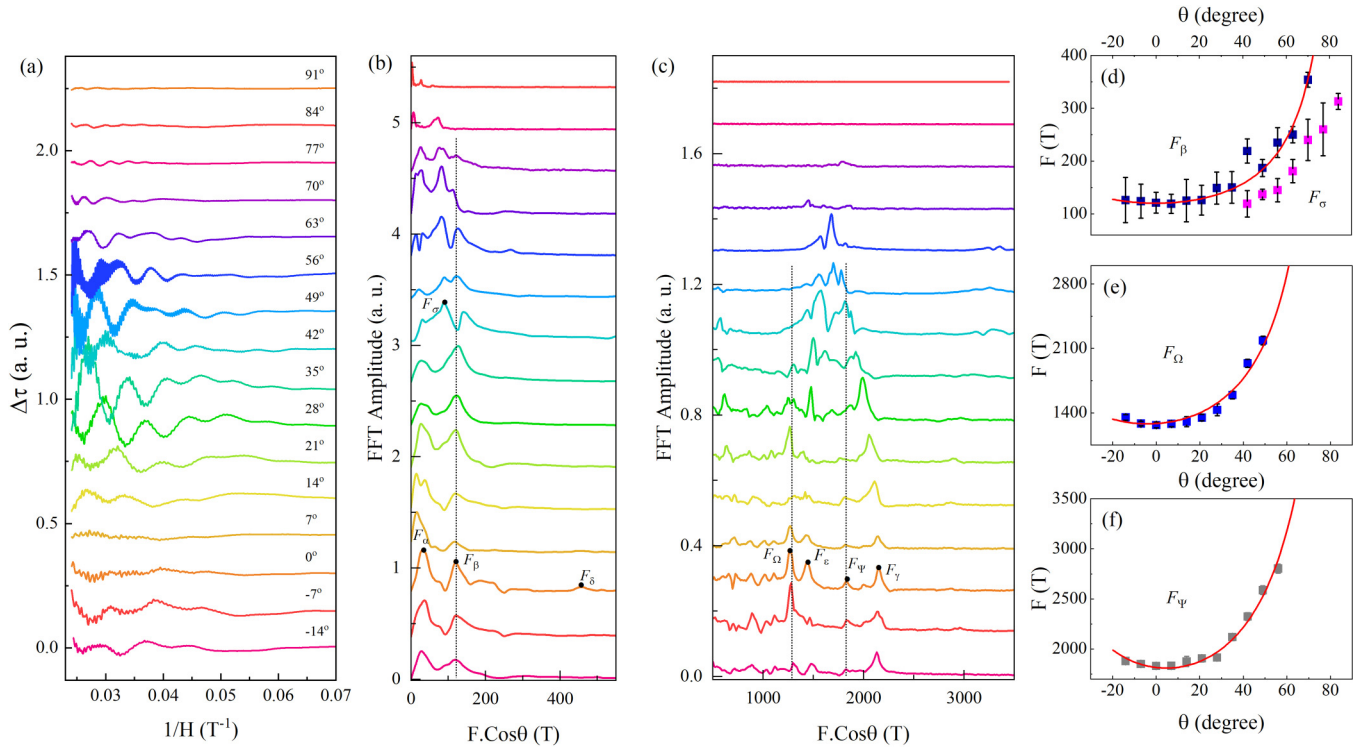


FIG. 3. Angular dependence of dHvA frequencies: (a) background-subtracted torque data for KV_3Sb_5 at selected θ 's at 0.32 K. The higher frequencies gradually disappear with increasing θ and are completely absent at 91° . FFT spectra in the ranges of (b) 0 to 500 T and (c) 500 to 3500 T. Note that the x axis is plotted as $F \cos \theta$. $F_\alpha \sim 39$ T in (b) is visible at all measured angles. Most of the peaks in (b) and (c) remain nearly unchanged as indicated by the vertical dot lines. Angular dependence of (d) F_σ and F_β , (e) F_Ω , and (f) F_Ψ . Frequencies can be clearly resolved up to 70° , and F_β , F_Ω , and F_Ψ show $1/\cos \theta$ dependence (solid red curves), which strongly suggests that their Fermi surfaces are 2D. The error bar for each data point is defined as the half-width at half maximum of the corresponding peak in the respective frequency spectrum.

we have selected K2 for further temperature and angle-dependence analyses. Figure 2(b) shows the background-subtracted torque data ($\Delta\tau$) for K2 at one of the measured angles $\theta = 0^\circ$. The oscillations are smooth and well defined. However, it appears that the signal is composed of multiple periods (and, hence, several frequencies), which is further evidenced in the frequency spectrum as shown in Figs. 2(c) and 2(d).

Figures 2(c) and 2(d) show the FFT spectrum of the dHvA oscillations data in the ranges of 0–600 T and 600–2400 T, respectively. There are 14 distinct frequency peaks, five of which are below 500 T ($F_\alpha = 33 \pm 21$, $F_\beta = 119 \pm 20$, $F_\chi = 194 \pm 25$, $F_\omega = 285 \pm 34$, and $F_\delta = 454 \pm 21$ T) and the remaining nine ($F_\lambda = 660 \pm 15$, $F_\rho = 881 \pm 20$, $F_\zeta = 1016 \pm 22$, $F_\mu = 1106 \pm 25$, $F_\Omega = 1267 \pm 30$, $F_\epsilon = 1430 \pm 27$, $F_\Psi = 1830 \pm 26$, $F_\xi = 2001 \pm 24$, and $F_\gamma = 2149 \pm 42$ T) of which are higher frequencies. It should be noted that there are additional peaks as indicated by daggers in Figs. 2(c) and 2(d) that are not clearly visible at other measured θ values. Even when they are visible, it is hard to determine their evolution with θ and identify their Fermi surfaces (to be discussed below). Therefore, we are not considering them as frequencies at this moment. These kinds of peaks were also observed in the FFT spectrum of CsV_3Sb_5 in our previous report [18] and in another report [16], and they were not considered as frequencies. Torque measurements under even higher fields might help to resolve the origin of these peaks. Two lower frequencies in KV_3Sb_5 , 34.6 and 148.9 T, were

reported by Yang *et al.* [9] based on their SdH oscillations, and those values are comparable to F_α and F_β , respectively, in our torque measurement data. However, the remaining 12 frequencies (F_χ , F_ω , F_δ , F_λ , F_ρ , F_ζ , F_μ , F_Ω , F_ϵ , F_Ψ , F_ξ , and F_γ) in KV_3Sb_5 are novel and have never previously been reported. Recently, we performed high-field torque measurements on CsV_3Sb_5 and along with other groups [16,18–22] have reported multiple quantum oscillation frequencies in this compound with values reaching as high as 10 kT. Therefore, the observation of higher frequencies in KV_3Sb_5 is consistent with that for CsV_3Sb_5 , and those frequencies likely have the same origin [16,19].

Angle-dependent dHvA oscillations provide information about the shape, size, and dimensionality of the Fermi surface [2,31]. Therefore, we rotated the sample *in situ* and measured the torque signal as a function of θ . Figure 3(a) shows the $\Delta\tau$ vs $1/H$ plot for KV_3Sb_5 at selected θ values. As can be seen in the figure, the period of the oscillations (and, hence, the frequency) changes with increasing θ . The lower frequencies are present at all θ values, whereas the higher frequencies gradually disappear above 63° . This is reflected in the FFT data shown in Figs. 3(b) and 3(c). Note the the x axis is plotted as $F \cos \theta$ to identify the scaling behavior of frequencies. Most of peaks are visible only up to 63° , and their positions remain nearly unchanged as indicated by the vertical dotted lines. This behavior strongly suggests that the observed frequencies scale with $1/\cos \theta$ and have 2D Fermi surfaces. F_α is present at all the measured θ values. Interestingly, the

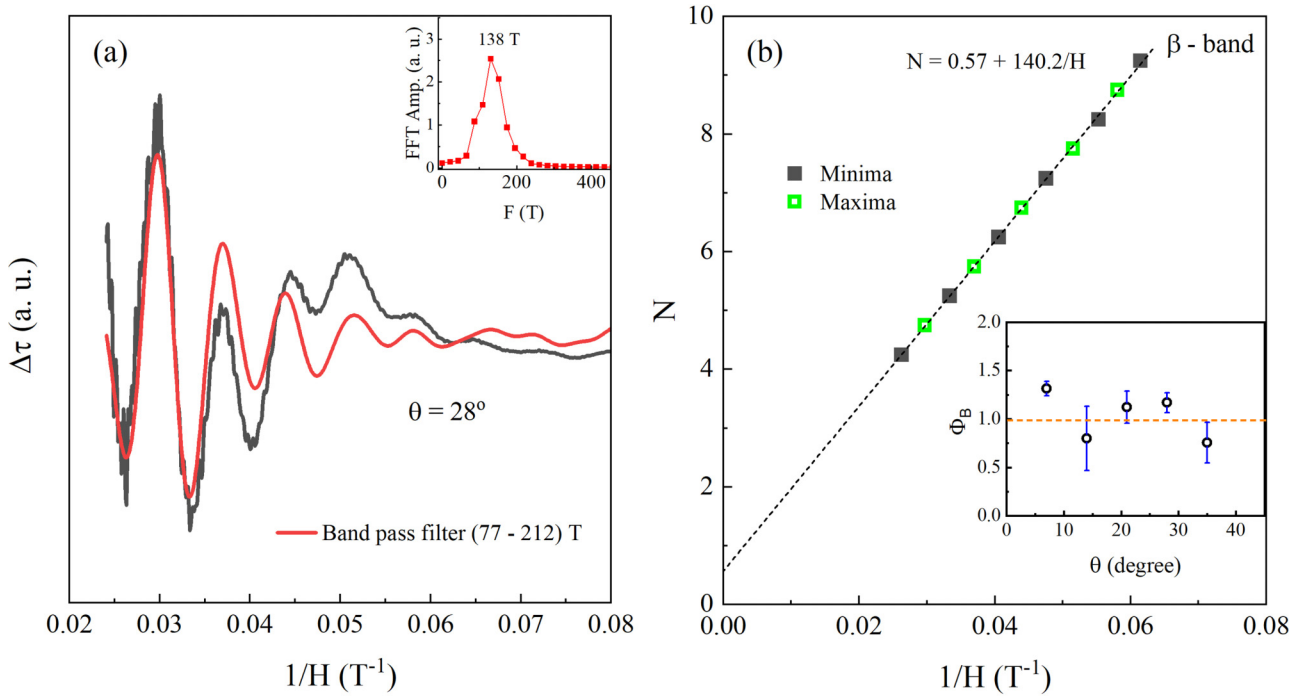


FIG. 4. Band-pass filter and Landau level (LL) fan diagram. (a) Separation of the dHvA oscillations corresponding to the β -band using the band-pass filter of (77–212 T). The black curve represents the raw data at $\theta = 28^\circ$, and the red curve is the filtered oscillation. The inset: FFT of the filtered signal. The existence of a single frequency at 138 T confirms that the filtered signal has oscillations only for F_β . (b) LL fan diagram for F_β . Minima and maxima of the oscillations were assigned to $(N + 1/4)$ and $(N - 1/4)$, respectively, for constructing the LL fan diagram. The dashed line is a linear extrapolation of the data in the limit $1/H \rightarrow 0$. The inset shows the Φ_B vs the θ plot up to 35° with a dashed line included as a guide for the eye.

previously unseen F_σ appears only above 42° , and it is visible up to 84° .

We noted that $F_\alpha = 33$ T does not show any systematic dependence on θ . Angular dependence of the frequency peak at 34.6 T for KV_3Sb_5 was also studied by Yang *et al.* [9] and they concluded that the 34.6-T pocket is not strictly 2D. The angular dependence of F_σ , F_β , F_Ω , and F_Ψ is shown in Figs. 3(d)–3(f). As expected, F_σ is present only in the short θ range of 42° – 84° . F_β increases with increasing θ and exhibits $1/\cos\theta$ behavior as shown by the solid red curve in Fig. 3(d). Similarly, F_Ω and F_Ψ (along with F_ϵ as shown in Fig. S3 in the Supplemental Material [23]) also exhibit $1/\cos\theta$ dependence [solid red curves in Figs. 3(e) and 3(f), respectively]. This strongly suggests that the Fermi surfaces of these frequencies (F_β , F_Ω , F_ϵ , and F_Ψ) are 2D [2,32,33]. The disappearance of these frequencies above $\theta = 63^\circ$ further confirms the 2D nature of their Fermi surfaces [2,34–36]. Our results regarding the angular dependence of frequencies in KV_3Sb_5 suggest the richness of quasi-2D Fermi surfaces in this compound. There have been a few recent reports of the existence of quasi-2D Fermi surfaces in CsV_3Sb_5 [16,18,19,21]. Therefore, the observation of quasi-2D Fermi surfaces in KV_3Sb_5 is consistent with previous findings for another AV_3Sb_5 compound.

From the analysis discussed above, we discovered that KV_3Sb_5 possesses several Fermi-surface pockets that are quasi-2D in nature. To understand the topological features of the Fermi surfaces, we calculated the Berry phase (Φ_B) by constructing a LL fan diagram [2,35,37,38]. Theoretically, Φ_B is π and 0 for topologically nontrivial and trivial

systems, respectively [2,33]. Due to the presence of multiple frequencies in KV_3Sb_5 , it would be challenging to separate quantum oscillations corresponding to individual frequencies and then construct a LL fan diagram. Therefore, we used a band-pass filter to separate the quantum oscillations from the raw data [39–43]. The black curve in Fig. 4(a) represents the raw data for dHvA oscillations at $\theta = 28^\circ$, and the red curve is the oscillation corresponding to F_β obtained using the band-pass filter of (77–212) T. The inset shows the FFT of the filtered oscillations. The presence of a single peak at 138 T confirms that the filtered signal has only one frequency (F_β). The assignment of the LL index for the torque data depends on the slope ($dF/d\theta$) of the frequency vs θ plot. For $dF/d\theta > 0$, the minima and maxima of the oscillations should be assigned to $(N + \frac{1}{4})$ and $(N - \frac{1}{4})$, respectively [18,37,42]. Since the frequencies in KV_3Sb_5 increase with θ (Fig. 3), i.e., $dF/d\theta > 0$, we assigned $(N + \frac{1}{4})$ for the minima and $(N - \frac{1}{4})$ for the maxima whereas constructing the LL fan diagram shown in Fig. 4(b).

From the linear extrapolation of the LL fan diagram data in the limit $1/H \rightarrow 0$, we have obtained the intercept (0.57 ± 0.01). This intercept value corresponds to $\Phi_B \sim \pi$, implying that F_β exhibits a nontrivial Fermi-surface topology. Based on the linear extrapolation, we have also obtained a slope equal to (140.2 ± 1.6) T, which is very close to the F_β frequency value of 138 T obtained from the FFT at $\theta = 28^\circ$ [the inset to Fig. 4(a)]. This confirms both that there is no significant error in determining the intercept (and, hence, the Φ_B value) using the linear extrapolation of the N vs $1/H$ data and that

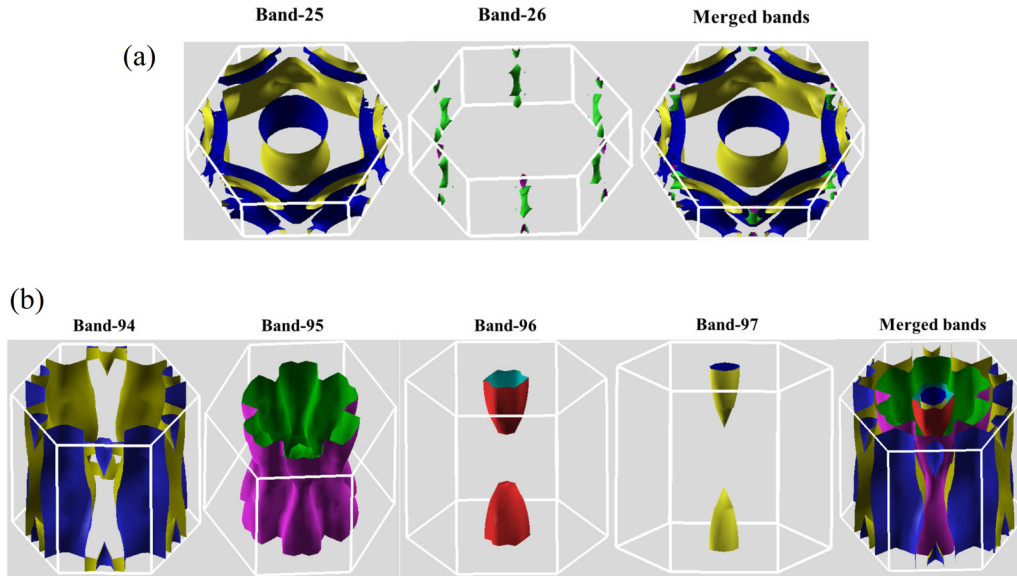


FIG. 5. DFT calculated Fermi-surface pieces. Band-resolved Fermi-surface pieces of the (a) pristine and (b) $2 \times 2 \times 1$ CDW phases of KV_3Sb_5 . The Fermi surface of the pristine unit cell displays a prominent 2D feature, including the cylinderlike Fermi surface centered around Γ and the large hexagonal Fermi surface in its vicinity. The heavily reconstructed Fermi-surface sheet resulting from distortion is seen in that of the CDW phase. The last image in both (a) and (b) shows the Fermi surface from all bands.

the band-pass filter preserves the original dHvA oscillation signal.

There have been reports [44–46] on some topological materials in which Φ_B changes with θ . As seen in Fig. 3(a), it appears that the positions of the maxima and minima change especially when rotating from $\theta = 28^\circ$ to 35° . Since the Φ_B value depends on the maxima and minima positions, we calculated Φ_B at a few angles near 28° by constructing an LL fan diagram as mentioned above. We found that although Φ_B changes slightly with θ , its value remains close to π as shown in the inset of Fig. 4(b). This further confirms the nontrivial topology of the β band. We did not calculate Φ_B at $\theta = 0^\circ$ nor above 35° due to the weak dHvA signal and the interference between F_σ and F_β , respectively.

To calculate the effective mass of the charge carriers, we carried out torque measurements at different temperatures in the range of 0.32 to 20 K and observed how the dHvA oscillations behave as temperature increases. This behavior can be explained by the Lifshitz-Kosevich (LK) formula [31,37,47]. The detailed LK analyses along with various physical parameters characterizing the Fermi-surface pockets are presented and tabulated in the Supplemental Material [23] (Figs. S4 and S5, and Table S2). As shown in Table S2 in the Supplemental Material [23], we observed that the effective mass (m^*) values of charge carriers in KV_3Sb_5 , $m^* \sim 0.8m_o$, are $m^* = 0.125m_o$ reported by Yang *et al.* [9] for KV_3Sb_5 and those for other family members RbV_3Sb_5 [9] and CsV_3Sb_5 [8,16,20]. However, they are comparable with those observed in recent studies on CsV_3Sb_5 [18,21,22]. It is important to note that the Fermi-surface parameters for KV_3Sb_5 presented here (Table S2 in the Supplemental Material [23]) are measured at $\theta = 49^\circ$. m^* and other relevant parameters might show angle dependence [48,49]. Systematic LK analyses at different θ 's are necessary to resolve this issue.

IV. COMPARISON WITH DFT CALCULATIONS

For comparison with the experimentally determined quantum oscillations frequencies, we also performed DFT calculations for both pristine and CDW phases of KV_3Sb_5 . Here, we focus on the trihexagonal (or inverse star-of-David) CDW phase, which is characterized by the in-plane ($2 \times 2 \times 1$) distortion of V atoms (see Fig. S6 in the Supplemental Material [23] for a comparison between the pristine and the CDW phases). This CDW phase is found to be slightly more energetically favorable by ~ 7 meV/unit cell in comparison to the pristine phase. We find that the CDW phase is in reasonable agreement with the measured quantum oscillation frequencies, which provides indirect evidence of the presence of the CDW phase.

Figures 5(a) and 5(b) show the Fermi surface of the pristine and $2 \times 2 \times 1$ CDW phases, respectively, of KV_3Sb_5 . The Fermi surface becomes reconstructed by the CDW pattern. Our results regarding the electronic band structure (Fig. S7 in the Supplemental Material [23]) and the Fermi surface are consistent with a previous report [19]. The theoretical Fermi surface cross-sectional areas were converted into oscillatory frequencies using the Onsager relation [50] for comparison with experimental results.

Table I shows the comparison between the calculated Fermi-surface frequencies for pristine and CDW phases along with some of the experimentally measured frequencies. Our results show that the Fermi-surface frequencies calculated from the CDW phase are in good agreement with those experimentally measured except for some higher frequencies greater than 4 kT. In addition, some experimentally observed frequencies especially frequencies from ~ 800 to 1800 T, could be not be explained from the DFT calculations. These discrepancies could be due to either the CDW phase not being the correct ground state or the inability of the experimental probe to

TABLE I. Comparison of theoretical and experimental quantum oscillation frequencies when the direction of the magnetic field is along the out-of-plane direction. Here, e and h denote electron and hole, respectively. The Fermi level for the CDW phase is shifted downward by 20 meV for better comparison with experiments.

Band	Pristine		CDW with $E_F - 20$ meV			Experimental $F(T)$
	$F(T)$	Orbit	Band	$F(T)$	Orbit	
25	169.00			32.40		33.00
	322.15			39.00		
	2402.15			207.06		194.00
	4454.28			404.95		454.00
	6139.07	h	94	583.29	h	
	6538.37			2111.75		2001.00
	7332.88			2129.29		2149.00
				4334.47		
26	58.13			109.50		119.00
	73.03		95	5500.98	e	
	196.73		96	593.06	e	660.00
	226.12	e	97	296.00	e	285.00
	376.90					

capture some frequency orbits. On the other hand, the pristine phase shows poor agreement with the experimental results. This provides an indirect justification of the presence of the CDW phase in this system.

V. SUMMARY

We have synthesized high-quality single crystals of KV_3Sb_5 , a member of the AV_3Sb_5 ($A = K, Rb, \text{ and } Cs$) kagome metal family and have determined its detailed Fermi-surface properties using the torque magnetometry technique. The torque signal under a DC magnetic field of 45 T and at the liquid 3He temperature (0.32 K) shows clear dHvA oscillations above 20 T. Similar to our findings from previous high-field studies on CsV_3Sb_5 [18], we observed 14 distinct peaks in the frequency spectrum, nine of which are above 500 T. The application of extremely high DC fields up to 45 T is helpful in tracking the angular variation of most of the frequencies observed here and unambiguously determining their Fermi-surface dimensionality. We discovered that F_β , F_Ω , F_ϵ , F_ψ , and F_γ show $1/\cos\theta$ dependence, where θ is the tilt angle of the applied field, confirming the quasi-2D Fermi surfaces of these frequencies. Furthermore, the Berry phase determined

by constructing the Landau level fan diagram is $\sim\pi$, strongly suggesting that the topology of KV_3Sb_5 is nontrivial.

The observation of higher frequencies above 500 T in KV_3Sb_5 is quite intriguing. To understand the origin of these frequencies, we also carried out DFT calculations on the KV_3Sb_5 electronic band structure and Fermi surfaces. Our DFT calculations confirmed that the Fermi surface of KV_3Sb_5 reconstructs in the CDW phase, and the oscillatory frequencies calculated from the cross-sectional areas of Fermi surfaces are comparable to quantum oscillation frequencies. There remain a few experimentally determined frequencies that could not be explained by the DFT calculations, and some high frequencies predicted by DFT are not observed in the quantum oscillations. This could be due to the CDW phase in DFT calculations not being the actual ground state or the inability of the experimental technique to capture some frequency orbits. Systematic DFT calculations and quantum oscillation studies at even higher magnetic fields might be helpful in resolving this issue. The detailed Fermi-surface information for KV_3Sb_5 and the corresponding DFT calculations presented here will be crucial in understanding the superconductivity, CDW order, and topological properties in this material and in the other AV_3Sb_5 family members CsV_3Sb_5 and RbV_3Sb_5 .

ACKNOWLEDGMENTS

The work at the West Texas A&M University is supported by the Killgore Faculty Research program, the KRC Undergraduate and Graduate Student Research Grants, and the Welch Foundation (Grant No. AE-0025). Work at the University of Houston was supported in part by the U.S. Air Force Office of Scientific Research Grants No. FA9550-15-1-0236 and No. FA9550-20-1-0068, the T. L. L. Temple Foundation, the John J. and Rebecca Moores Endowment, and the State of Texas through the Texas Center for Superconductivity at the University of Houston. The work at Hefei National Laboratory for Physical Sciences at the Microscale, University of Science and Technology of China, is supported by the Strategic Priority Research Program of the Chinese Academy of Sciences (Grant No. XDB25000000) and the National Natural Science Foundation of China (Grant No. 11888101). A portion of this work was performed at the National High Magnetic Field Laboratory, which was supported by National Science Foundation Cooperative Agreement No. DMR-1644779 and the State of Florida.

- [1] B. R. Ortiz, L. C. Gomes, J. R. Morey, M. Winiarski, M. Bordelon, J. S. Mangum, I. W. H. Oswald, J. A. Rodriguez-Rivera, J. R. Neilson, S. D. Wilson, E. Ertekin, T. M. McQueen, and E. S. Toberer, New kagome prototype materials: Discovery of KV_3Sb_5 , RbV_3Sb_5 , and CsV_3Sb_5 , *Phys. Rev. Mater.* **3**, 094407 (2019).
- [2] B. R. Ortiz, P. M. Sarte, E. M. Kenney, M. J. Graf, S. M. L. Teicher, R. Seshadri, and S. D. Wilson, Superconductivity in the Z_2 kagome metal KV_3Sb_5 , *Phys. Rev. Mater.* **5**, 034801 (2021).
- [3] B. R. Ortiz, S. M. L. Teicher, Y. Hu, J. L. Zuo, P. M. Sarte, E. C. Schueller, A. M. M. Abeykoon, M. J. Krogstad, S. Rosenkranz, R. Osborn, R. Seshadri, L. Balents, J. He, and S. D. Wilson, CsV_3Sb_5 : Az_2 Topological Kagome Metal with a Superconducting Ground State, *Phys. Rev. Lett.* **125**, 247002 (2020).
- [4] K. Jiang, T. Wu, J.-X. Yin, Z. Wang, M. Z. Hasan, S. D. Wilson, X. Chen, and J. Hu, Kagome superconductors AV_3Sb_5 ($A=K, Rb, Cs$), *Natl. Sci. Rev.* **10**, nwac199 (2023).

- [5] F. H. Yu, D. H. Ma, W. Z. Zhuo, S. Q. Liu, X. K. Wen, B. Lei, J. J. Ying, and X. H. Chen, Unusual competition of superconductivity and charge-density-wave state in a compressed topological kagome metal, *Nat. Commun.* **12**, 3645 (2021).
- [6] K. Y. Chen, N. N. Wang, Q. W. Yin, Y. H. Gu, K. Jiang, Z. J. Tu, C. S. Gong, Y. Uwatoko, J. P. Sun, H. C. Lei, J. P. Hu, and J.-G. Cheng, Double Superconducting Dome and Triple Enhancement of T_c in the Kagome Superconductor CsV_3Sb_5 Under High Pressure, *Phys. Rev. Lett.* **126**, 247001 (2021).
- [7] N. N. Wang, K. Y. Chen, Q. W. Yin, Y. N. N. Ma, B. Y. Pan, X. Yang, X. Y. Ji, S. L. Wu, P. F. Shan, S. X. Xu, Z. J. Tu, C. S. Gong, G. T. Liu, G. Li, Y. Uwatoko, X. L. Dong, H. C. Lei, J. P. Sun, and J.-G. Cheng, Competition between charge-density-wave and superconductivity in the kagome metal RbV_3Sb_5 , *Phys. Rev. Res.* **3**, 043018 (2021).
- [8] F. H. Yu, T. Wu, Z. Y. Wang, B. Lei, W. Z. Zhuo, J. J. Ying, and X. H. Chen, Concurrence of anomalous Hall effect and charge density wave in a superconducting topological kagome metal, *Phys. Rev. B* **104**, L041103 (2021).
- [9] S.-Y. Yang, Y. Wang, B. R. Ortiz, D. Liu, J. Gayles, E. Derunova, R. Gonzalez-Hernandez, L. Šmejkal, Y. Chen, S. S. P. Parkin, S. D. Wilson, E. S. Toberer, and T. M. M. N. Ali, Giant, unconventional anomalous Hall effect in the metallic frustrated magnet candidate, KV_3Sb_5 , *Sci. Adv.* **6** (2020).
- [10] M. Kang, S. Fang, J. K. Kim, B. R. Ortiz, S. H. Ryu, J. Kim, J. Yoo, G. Sangiovanni, D. D. Sante, B. G. Park, C. Jozwiak, A. Bostwick, E. Rotenberg, E. Kaxiras, S. D. Wilson, J. H. Park, and R. Comin, Twofold van hove singularity and origin of charge order in topological kagome superconductor CsV_3Sb_5 , *Nat. Phys.* **18**, 301 (2022).
- [11] Z. Liang, X. Hou, F. Zhang, W. Ma, P. Wu, Z. Zhang, F. Yu, J.-J. Ying, K. Jiang, L. Shan, Z. Wang, and X.-H. Chen, Three-Dimensional Charge Density Wave and Surface-Dependent Vortex-Core States in a Kagome Superconductor CsV_3Sb_5 , *Phys. Rev. X* **11**, 031026 (2021).
- [12] L. Nie, K. Sun, W. Ma, D. Song, L. Zheng, Z. Liang, P. Wu, F. Yu, J. Li, M. Shan, D. Zhao, S. Li, B. Kang, Z. Wu, Y. Zhou, K. Liu, Z. Xiang, J. Ying, Z. Wang, T. Wu, and X. Chen, Charge-density-wave-driven electronic nematicity in a kagome superconductor, *Nature (London)* **604**, 59 (2022).
- [13] C. M. III, D. Das, J.-X. Yin, H. Liu, R. Gupta, Y.-X. Jiang, M. Medarde, X. Wu, H. C. Lei, J. Chang, P. Dai, Q. Si, H. Miao, R. Thomale, T. Neupert, Y. Shi, R. Khasanov, M. Z. Hasan, H. Luetkens, and Z. Guguchi, Time-reversal symmetry-breaking charge order in a kagome superconductor, *Nature (London)* **602**, 245 (2022).
- [14] Q. Yin, Z. Tu, C. Gong, Y. Fu, S. Yan, and H. Lei, Superconductivity and normal-state properties of kagome metal RbV_3Sb_5 single crystals, *Chin. Phys. Lett.* **38**, 037403 (2021).
- [15] K. Nakayama, Y. Li, T. Kato, M. Liu, Z. Wang, T. Takahashi, Y. Yao, and T. Sato, Carrier Injection and Manipulation of Charge-Density Wave in Kagome Superconductor CsV_3Sb_5 , *Phys. Rev. X* **12**, 011001 (2022).
- [16] B. R. Ortiz, S. M. L. Teicher, L. Kautzsch, P. M. Sarte, N. Ratcliff, J. Harter, J. P. C. Ruff, R. Seshadri, and S. D. Wilson, Fermi Surface Mapping and the Nature of Charge Density Wave Order in the Kagome Superconductor CsV_3Sb_5 , *Phys. Rev. X* **11**, 041030 (2021).
- [17] H. Luo, Q. Gao, H. Liu, Y. Gu, D. Wu, C. Yi, J. Jia, S. Wu, X. Luo, Y. Xu, L. Zhao, Q. Wang, H. Mao, G. Liu, Z. Zhu, Y. Shi, K. Jiang, J. Hu, Z. Xu, and X. J. Zhou, Electronic nature of charge density wave and electron-phonon coupling in kagome superconductor KV_3Sb_5 , *Nat. Commun.* **13**, 273 (2022).
- [18] K. Shrestha, R. Chapai, B. K. Pokharel, D. Miertschin, T. Nguyen, X. Zhou, D. Y. Chung, M. G. Kanatzidis, J. F. Mitchell, U. Welp, D. Popović, D. E. Graf, B. Lorenz, and W. K. Kwok, Nontrivial Fermi surface topology of the kagome superconductor CsV_3Sb_5 probed by de Haas–van Alphen oscillations, *Phys. Rev. B* **105**, 024508 (2022).
- [19] Y. Fu, N. Zhao, Z. Chen, Q. Yin, Z. Tu, C. Gong, C. Xi, X. Zhu, Y. Sun, K. Liu, and H. Lei, Quantum Transport Evidence of Topological Band Structures of Kagome Superconductor CsV_3Sb_5 , *Phys. Rev. Lett.* **127**, 207002 (2021).
- [20] R. Chapai, M. Leroux, V. Oliviero, D. Vignolles, M. P. Smylie, D. Y. Chung, M. G. Kanatzidis, W.-K. Kwok, J. F. Mitchell, and U. Welp, Magnetic Breakdown and Topology in the Kagome Superconductor CsV_3Sb_5 Under High Magnetic Field, *Phys. Rev. Lett.* **130**, 126401 (2023).
- [21] W. Zhang, L. Wang, C. W. Tsang, X. Liu, J. Xie, W. C. Yu, K. T. Lai, and S. K. Goh, Emergence of large quantum oscillation frequencies in thin flakes of the kagome superconductor CsV_3Sb_5 , *Phys. Rev. B* **106**, 195103 (2022).
- [22] C. Broyles, D. Graf, H. Yang, X. Dong, H. Gao, and S. Ran, Effect of the Interlayer Ordering on the Fermi Surface of Kagome Superconductor CsV_3Sb_5 Revealed by Quantum Oscillations, *Phys. Rev. Lett.* **129**, 157001 (2022).
- [23] See Supplemental Material at <http://link.aps.org/supplemental/10.1103/PhysRevB.107.155128> for detailed information on EDX, comparison of frequencies, angle-dependent frequency data, dingle temperature analyses, etc.
- [24] G. Kresse and J. Hafner, *Ab initio* molecular dynamics for liquid metals, *Phys. Rev. B* **47**, 558 (1993).
- [25] P. E. Blöchl, Projector augmented-wave method, *Phys. Rev. B* **50**, 17953 (1994).
- [26] J. P. Perdew, K. Burke, and M. Ernzerhof, Generalized Gradient Approximation Made Simple, *Phys. Rev. Lett.* **77**, 3865 (1996).
- [27] V. Popescu and A. Zunger, Extracting E versus \vec{k} effective band structure from supercell calculations on alloys and impurities, *Phys. Rev. B* **85**, 085201 (2012).
- [28] <https://github.com/QijingZheng/VaspBandUnfolding>.
- [29] A. Kokalj, XCrySDen—a new program for displaying crystalline structures and electron densities, *J. Mol. Graph. Modell.* **17**, 176 (1999).
- [30] P. Rourke and S. Julian, Numerical extraction of de Haas–van Alphen frequencies from calculated band energies, *Comput. Phys. Commun.* **183**, 324 (2012).
- [31] K. Shrestha, *Magnetotransport Studies on Topological Insulators*, Doctoral dissertation, University of Houston, 2015.
- [32] D.-X. Qu, Y. S. Hor, J. Xiong, R. J. Cava, and N. P. Ong, Quantum oscillations and hall anomaly of surface states in the topological insulator Bi_2Te_3 , *Science* **329**, 821 (2010).
- [33] K. Shrestha, V. Marinova, B. Lorenz, and C. W. Chu, Evidence of a 2d fermi surface due to surface states in a p-type metallic Bi_2Te_3 , *J. Phys.: Condens. Matter* **30**, 185601 (2018).
- [34] K. Shrestha, V. Marinova, B. Lorenz, and P. C. W. Chu, Shubnikov-de Haas oscillations from topological surface states of metallic $Bi_2Se_{2.1}Te_{0.9}$, *Phys. Rev. B* **90**, 241111(R) (2014).
- [35] K. Shrestha, D. E. Graf, V. Marinova, B. Lorenz, and P. C. W. Chu, Simultaneous detection of quantum oscillations from bulk

- and topological surface states in metallic $\text{Bi}_2\text{Se}_{2.1}\text{Te}_{0.9}$, *Philos. Mag.* **97**, 1740 (2017).
- [36] J. G. Analytis, R. D. McDonald, S. C. Riggs, J.-H. Chu, G. S. Boebinger, and I. R. Fisher, Two-dimensional surface state in the quantum limit of a topological insulator, *Nat. Phys.* **6**, 960 (2010).
- [37] D. Shoenberg, *Magnetic Oscillations in Metals* (Cambridge University Press, Cambridge, UK, 1984).
- [38] K. Shrestha, D. Miertschin, R. Sankar, B. Lorenz, and C. W. Chu, Large magnetoresistance and quantum oscillations in $\text{Sn}_{0.05}\text{Pb}_{0.95}\text{Te}$, *J. Phys.: Condens. Matter* **33**, 335501 (2021).
- [39] W. Zheng, R. Schönemann, N. Aryal, Q. Zhou, D. Rhodes, Y.-C. Chiu, K.-W. Chen, E. Kampert, T. Förster, T. J. Martin, G. T. McCandless, J. Y. Chan, E. Manousakis, and L. Balicas, Detailed study of the fermi surfaces of the type-II dirac semimetallic candidates XTe_2 ($\text{X}=\text{Pd}, \text{Pt}$), *Phys. Rev. B* **97**, 235154 (2018).
- [40] W. Zheng, R. Schönemann, S. Mozaffari, Y.-C. Chiu, Z. B. Goraum, N. Aryal, E. Manousakis, T. M. Siegrist, K. Wei, and L. Balicas, Bulk fermi surfaces of the dirac type-II semimetallic candidate NiTe_2 , *Phys. Rev. B* **102**, 125103 (2020).
- [41] M. A. Khan, D. E. Graf, I. Vekhter, D. A. Browne, J. F. DiTusa, W. A. Phelan, and D. P. Young, Quantum oscillations and a nontrivial berry phase in the noncentrosymmetric topological superconductor candidate BiPd , *Phys. Rev. B* **99**, 020507(R) (2019).
- [42] R. Chapai, D. A. Browne, D. E. Graf, J. F. DiTusa, and R. Jin, Quantum oscillations with angular dependence in PdTe_2 single crystals., *J. Phys.: Condens. Matter* **33**, 035601 (2021).
- [43] T. Nguyen, N. Aryal, B. K. Pokharel, L. Harnagea, D. Mierstchin, D. Popović, D. E. Graf, and K. Shrestha, Fermiology of the dirac type-II semimetal candidates $(\text{Ni}, \text{Zr})\text{Te}_2$ using de Haas-van Alphen oscillations, *Phys. Rev. B* **106**, 075154 (2022).
- [44] K. Zhang, Y. Du, P. Wang, L. Wei, L. Li, Q. Zhang, W. Qin, Z. Lin, B. Cheng, Y. Wang *et al.*, Butterfly-like anisotropic magnetoresistance and angle-dependent berry phase in a type-II Weyl Semimetal WP_3 , *Chin. Phys. Lett.* **37**, 090301 (2020).
- [45] M. N. Ali, L. M. Schoop, C. Garg, J. M. Lippmann, E. Lara, B. Lotsch, and S. S. Parkin, Butterfly magnetoresistance, quasi-2d Dirac Fermi surface and topological phase transition in ZrSiS , *Sci. Adv.* **2**, e1601742 (2016).
- [46] Z. J. Xiang, D. Zhao, Z. Jin, C. Shang, L. K. Ma, G. J. Ye, B. Lei, T. Wu, Z. C. Xia, and X. H. Chen, Angular-Dependent Phase Factor of Shubnikov-de Haas Oscillations in the Dirac Semimetal Cd_3As_2 , *Phys. Rev. Lett.* **115**, 226401 (2015).
- [47] K. Shrestha, V. Marinova, D. Graf, B. Lorenz, and C. W. Chu, Quantum oscillations in metallic $\text{Sb}_2\text{Te}_2\text{Se}$ topological insulator, *Phys. Rev. B* **95**, 075102 (2017).
- [48] F. Wu, C. Y. Guo, M. Smidman, J. L. Zhang, and H. Q. Yuan, Large magnetoresistance and Fermi surface topology of PrSb , *Phys. Rev. B* **96**, 125122 (2017).
- [49] J. Wosnitzer, G. W. Crabtree, H. H. Wang, K. D. Carlson, M. D. Vashon, and J. M. Williams, Angular Dependence of the Cyclotron Effective Mass in Organic Superconductors, *Phys. Rev. Lett.* **67**, 263 (1991).
- [50] According to the Onsager's relation, the quantum oscillation measured frequency of an electron orbit (F) which is perpendicular to the applied magnetic field is related to the area of the Fermi surface (A) by $F = \frac{\phi_0}{2\pi^2}A$ where $\phi_0 = 2.07 \times 10^{-15} \text{ Tm}^2$ is the quantum of flux.